Front. Chem. Sci. Eng. 2012, 6(4): 371–380
DOI 10.1007/s11705-012-1215-3

RESEARCH ARTICLE

# Comparison of the morphology and structure of $WO_3$ nanomaterials synthesized by a sol-gel method followed by calcination or hydrothermal treatment

**Diah Susanti (✉)[1], Stefanus Haryo N[1], Hasnan Nisfu[1], Eko Prasetio Nugroho[1], Hariyati Purwaningsih[1], George Endri Kusuma[2], Shao-Ju Shih[3]**

1 Materials and Metallurgical Engineering Department, Faculty of Industrial Technology, Sepuluh Nopember Institute of Technology (ITS), Surabaya 60111, Indonesia
2 Mechanical Engineering Department, Surabaya State Shipbuilding Polytechnic, Surabaya 60111, Indonesia
3 Materials Science and Engineering Department, Taiwan Tech (NTUST), Taipei 106, China



**Abstract** Tungsten (VI) oxide ($WO_3$) nanomaterials were synthesized by a sol-gel method using $WCl_6$ and $C_2H_5OH$ as precursors followed by calcination or hydrothermal treatment. X-Ray diffraction (XRD), scanning electron microscopy (SEM) and high resolution transmission electron microscopy (HRTEM) equipped with energy dispersive X-ray spectroscopy (EDX) were used to characterize the structure and morphology of the materials. There were significant differences between the $WO_3$ materials that were calcinated and those that were subjected to a hydrothermal process. The XRD results revealed that calcination temperatures of 300°C and 400°C gave hexagonal structures and temperatures of 500°C and 600°C gave monoclinic structures. The SEM images showed that an increase in calcination temperature led to a decrease in the $WO_3$ powder particle size. The TEM analysis showed that several nanoparticles agglomerated to form bigger clusters. The hydrothermal process produced hexagonal structures for holding times of 12, 16, and 20 h and monoclinic structures for a holding time of 24 h. The SEM results showed transparent rectangular particles which according to the TEM results originated from the aggregation of several nanotubes.

**Keywords** $WO_3$ nanomaterial, sol-gel method, calcination, hydrothermal

Received April 17, 2012; accepted July 13, 2012

E-mail: santiche@mat-eng.its.ac.id

## 1 Introduction

Tungsten oxides are semiconductor metal oxide materials that have band gaps in the range of 2.6–3.0 eV. Since tungsten metal has several oxidation numbers, tungsten oxide forms different compounds, such as $W_3O$ [1], $WO_2$, $WO_{2.72}$, $WO_{2.9}$, $WO_{2.96}$, and $WO_3$ in which the oxidation states of tungsten range from + 0.67 to + 6 [2]. One which has attracted much attention is tungsten (VI) oxide or tungsten trioxide ($WO_3$). $WO_3$ materials have a wide range of applications in gas sensors [3–8], electrochromic devices [9], electrochemical capacitors [10], photocatalysts [11], optical devices [12] and smart windows [13]. The structure, surface morphology, particle size distribution, defect structure and active surface area of the $WO_3$ material greatly influence its properties including its sensing, electrochromic, catalytic, optical, and capacitive properties.

Many methods have been used to synthesize $WO_3$, such as sol-gel methods [6,10,14,15], metal organic chemical vapor deposition (MOCVD) [16], reactive sputtering [17], a colloidal gas aphrons method [18], spray pyrolisis [11], flame-based solid evaporation [19], liquid phase deposition [20] and solvothermal synthesis [21]. Among these methods, the sol-gel method is cheap, simple and easy and does not require strict controls on pressure and temperature. In addition, it is also applicable for the mass production of thin or thick films.

Sols and gels are two forms of colloids. A sol is a colloidal suspension of solid particles in a liquid, whereas a gel is a colloidal suspension of liquid droplets in a solid. A sol-gel process involves a transition from an "aqueous" sol form to a "solid" gel form. In the sol-gel process, the

precursors (starting compounds) for the preparation of a colloid consist of a metal or metalloid element surrounded by various ligands. For example, common precursors for tungsten oxide include inorganic salts, such as $WCl_6$ and organic compounds such as $W(OC_2H_5)$. The latter are called alkoxides and are the class of precursors most widely used in sol-gel research. An alkoxide can be prepared by reacting an inorganic salt with an alcohol. For example, $W(OC_2H_5)$ can be obtained by reacting the inorganic salt $WCl_6$ with ethanol. An acid or base catalyst such as $NH_4OH$, $HNO_3$ or $H_2SO_4$ is usually added to influence the hydrolysis and condensation rates and the structure of the condensed product [22].

Most gels are amorphous, even after drying, but many crystallize when heated. Therefore high temperature calcination and hydrothermal processes are frequently used to obtain crystalline nanomaterials after a sol-gel process. Calcination is a thermal treatment process that affects thermal decomposition, phase transitions, structure formation, and removal of volatile materials. Hydrothermal processes utilize pressurized steam to crystallize and form the desired shape, size and structure of the nanomaterial. It works at relatively low temperatures, is simple to operate and results in high sample homogeneity and quality. However it takes a longer time to carry out the process than calcination does. Recently hydrothermal processes carried out in a microwave device have helped in reducing the time without reducing the quality of the synthesized material [10,21].

Various precursors such as ammonium metatungstate $[(NH_4)_{10}W_{12}O_{41}\cdot xH_2O]$ [5,15], $WCl_6$ [6], $Na_2WO_4\cdot 2H_2O$ [10], $WOCl_4$ [15], and $Na_2WO_4$ [23] have been employed to synthesize $WO_3$ nanomaterials via sol-gel methods. Each precursor results in a different structure and morphology of $WO_3$ which effect how the material can be applied. According to Wang et al. [6], a $WO_3$ nanocrystalline material produced by tungsten alkoxide $W(OR)_6$ from a $WCl_6$ precursor showed good sensing performances for $O_3$ and $NO_2$. In addition, the synthesis of $WO_3$ by a sol-gel process using $WCl_6$ as the precursor required a relatively short time (a maximum of 24 h) compared to that when tungsten metatungstate was used as the precursor [24] (which needed a week).

Wang et al. [6] synthesized $WO_3$ via a sol-gel method using a $WCl_6$ precursor and calcined the gel which had been spin-coated on top of alumina wafers at different temperatures (350°C–650°C) for 1 h. Although many papers have reported hydrothermal processes on $WO_3$, which has been prepared from various precursors, there are few papers that have reported the application of a hydrothermal method to produce $WO_3$ nanomaterials from a sol-gel method using a $WCl_6$ precursor. Therefore, this paper reports the synthesis of $WO_3$ nanomaterials via a sol-gel method using $WCl_6$ and $C_2H_5OH$ as the precursors followed by calcination or hydrothermal treatment. X-Ray diffraction (XRD), scanning electron microscopy (SEM) and high resolution transmission electron microscopy (HRTEM) were used to characterize and compare the structures and morphologies of the resulting nanomaterials. Energy dispersive X-ray spectroscopy (EDX) was used to analyze the chemical composition of the materials.

## 2 Experimental methods

### 2.1 $WO_3$ synthesis by sol-gel process

A sol–gel process adopted from Wang et al. [6] was used to produce tungsten (VI) oxide ($WO_3$) nanomaterials. The tungsten alkoxide precursor was prepared by first mixing 7 g of tungsten (VI) hexachloride ($WCl_6$) (Acros Organics) with 100 mL of ethanol ($C_2H_5OH$) (Merck). Then 10 mL of 0.5 $mol\cdot L^{-1}$ ammonia hydroxide ($NH_4OH$) solution was added dropwise to the precursor solution and stirred for 24 h under ice cooling to carry out the hydrolysis and condensation processes. The chloride ions were removed from the precipitate by washing with de-ionized-water and centrifuging until no white AgCl precipitate appeared when titrated with 0.1 $mol\cdot L^{-1}$ silver nitrate solution. The washed precipitate was then peptized with a solution of ammonia hydroxide and 50 μL of surfactant (Triton X-100). In this batch process, 100 mL of tungsten trioxide containing sol was obtained.

### 2.2 Thermal treatments

Two different thermal treatments were used to obtain nanocrystalline $WO_3$: calcination and hydrothermal treatment. For the calcination, the $WO_3$ gel was placed in a covered alumina crucible and calcined in a furnace under atmospheric air at 300°C, 400°C, 500°C or 600°C for 1 h.

For the hydrothermal treatment, the $WO_3$ gel was placed in a 50 mL-Teflonlined stainless steel autoclave and heated in a furnace under atmospheric air at 200°C for 12, 16, 20 or 24 h. In addition, the gel was heated at different temperatures (160°C, 180°C, and 200°C) for 12 h. The wet sample from the hydrothermal treatment was dried at 100°C for 1 h to remove the moisture.

For both types of thermal treatments the samples were slowly cooled to room temperature in the furnace. This method allows the particles to become well ordered and results in crystalline solids.

### 2.3 Material characterization

The surface morphology and particle size of tungsten oxide were examined using scanning electron microscopy (Zeiss EVO MA 10), transmission electron microscopy (JEOL JSM-1400) and high resolution transmission electron microscopy (FEI Tecnai $G^2$) with energy dispersive X-ray spectroscopy for chemical analysis. The particle sizes in the $WO_3$ powder were measured by using the SEM or

HRTEM scale bars. The crystalline structure and crystallite sizes were determined using X-ray diffraction measurements (Philips X-Pert XMS) with a Cu Kα source with a wavelength of 1.54056 Å.

## 3 Results and discussion

The color of the $WO_3$ powder depended on the calcination temperature and on the hydrothermal holding time. The calcinated powders were brown, dark brown, green or greenish yellow at 300°C, 400°C, 500°C and 600°C respectively; and were dark blue or blue for hydrothermal holding times of 12 – 16 h and 20 – 24 h, respectively. In terms of particle size, a higher calcination temperature was more effective in eliminating large agglomerates in the powder, resulting in finer and looser powders; and a prolonged hydrothermal holding time increased the amount of granular powder.

Figure 1 shows the secondary electron SEM images of the $WO_3$ nanomaterial surfaces after calcination at 300°C, 400°C, 500°C and 600°C. Obviously the $WO_3$ nanoparticles have grainy shapes and tend to form aggregations. As seen in Fig. 1(a) a cluster (which appears as a circle), consists of 8–20 small particles. However, as the temperature increased, the aggregation and particle sizes tended to decrease. At lower temperatures, the water molecules, other volatile materials such as HCl, $C_2H_5OH$, and $NH_4OH$, and the surfactant bond to some $WO_3$ particles to make clusters. At higher temperatures, these substances are vaporized and removed from the $WO_3$ powder and hence the amount of aggregation and particle sizes were reduced.

Houx et al. [21] reported the same trend of particle sizes decreasing with increasing synthesis temperature. Wang et al. [6] also obtained the same shapes of $WO_3$ nanomaterials as shown in Fig. 1, but their particle sizes tended to increase with increasing temperature since their materials were spin-coated on top of alumina wafers for sensor applications.

Figure 2 shows the secondary electron SEM images of $WO_3$ nanomaterials after hydrothermal treatment at 200°C with holding times of 12, 16, 20, and 24 h. These results are different from those shown in Fig. 1. In Fig. 2(a), the

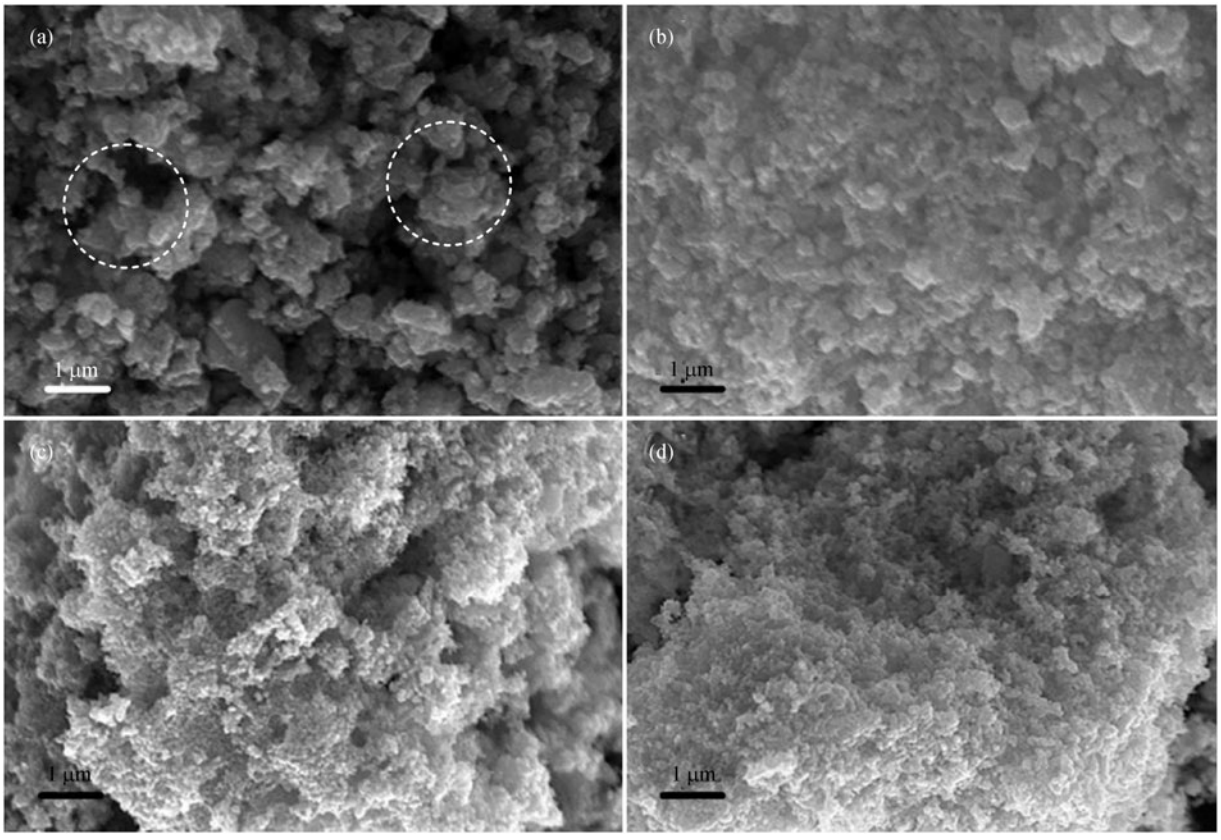


**Fig. 1** Secondary electron SEM images of $WO_3$ nanomaterials after calcination at different temperatures (a) 300°C, particle sizes: 277–780 nm, (b) 400°C, particle sizes: 137–550 nm, (c) 500°C, particle sizes: 50–500 nm and (d) 600°C, particle sizes: 25–125 nm. The circles indicate clusters of particles

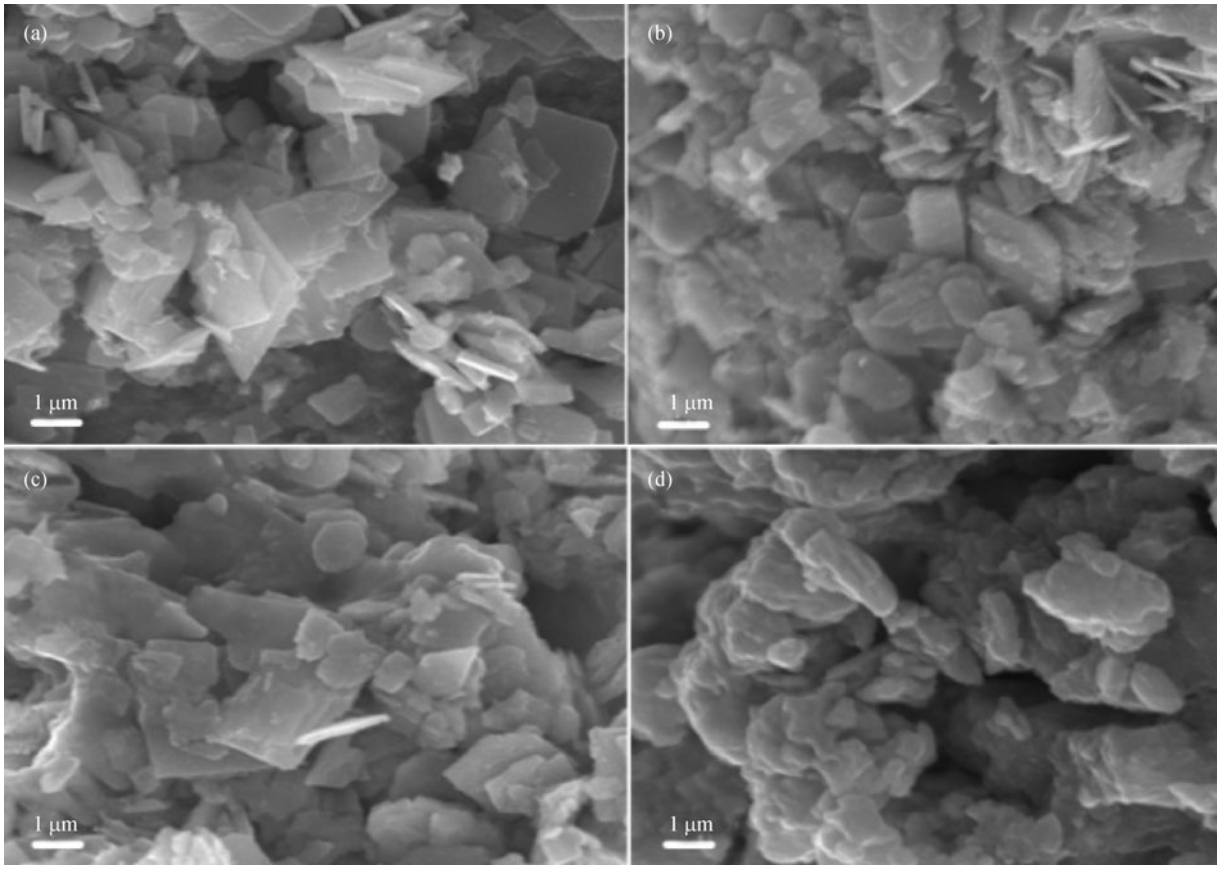


**Fig. 2** Secondary electron SEM images of $WO_3$ nanomaterials after hydrothermal treatment at 200°C for holding times of (a) 12 h, (b) 16 h, (c) 20 h, and (d) 24 h

$WO_3$ nanomaterials have thin rectangular shaped transparent flakes with particle sizes of 0.4–3 μm and thicknesses of ~ 100 nm. As the holding time increased the particle size and thickness became larger and therefore the particles formed aggregates and finally lost their shapes at a holding time of 24 h as shown in Fig. 2(d). Because of the reaction kinetics, prolonging the reaction time helped the solid particles grow larger. The particle sizes and thicknesses are listed in Table 1.

The SEM images of the $WO_3$ synthesized by a sol-gel method followed by hydrothermal treatment at 160°C, 180°C, or 200°C for 12 h is shown in Fig. 3. The shapes of the materials are similar to those in Fig. 2. The rectangular flakes became bigger as the temperature increased. This is expected since higher temperatures give more energy for solid particles to grow. The sizes and thicknesses of the particles are shown in Table 2.

Figure 4 shows the XRD patterns of the $WO_3$ nanomaterials after calcination at 300°C, 400°C, 500°C or 600°C. The structure is hexagonal at 300°C and 400°C and changes to monoclinic at 500°C and 600°C. The crystalline planes were identified using JCPDS hexagonal card No. 85-2459 [25] with corresponding lattice parameters of $a = b = 7.324$ Å and $c = 7.662$ Å and monoclinic

**Table 1** $WO_3$ nanomaterials particle sizes after hydrothermal treatment at 200°C with different holding times

| Holding time/h | 12 | 16 | 20 | 24 |
|---|---|---|---|---|
| Particle size/μm | 0.4–3 | 0.4–3.5 | 0.5–4 | 0.5–4.2 |
| Particle thickness/nm | ~ 100 | ~ 150 | ~ 200 | ~ 300 |

**Table 2** Particle sizes of $WO_3$ nanomaterials after hydrothermal treatment at different temperatures with a holding time of 12 h

| Temperature/°C | 160 | 180 | 200 |
|---|---|---|---|
| Particle size/μm | 0.4–2 | 0.4–2.2 | 0.4–3 |
| Particle thickness/nm | ~ 70 | ~ 90 | ~ 100 |

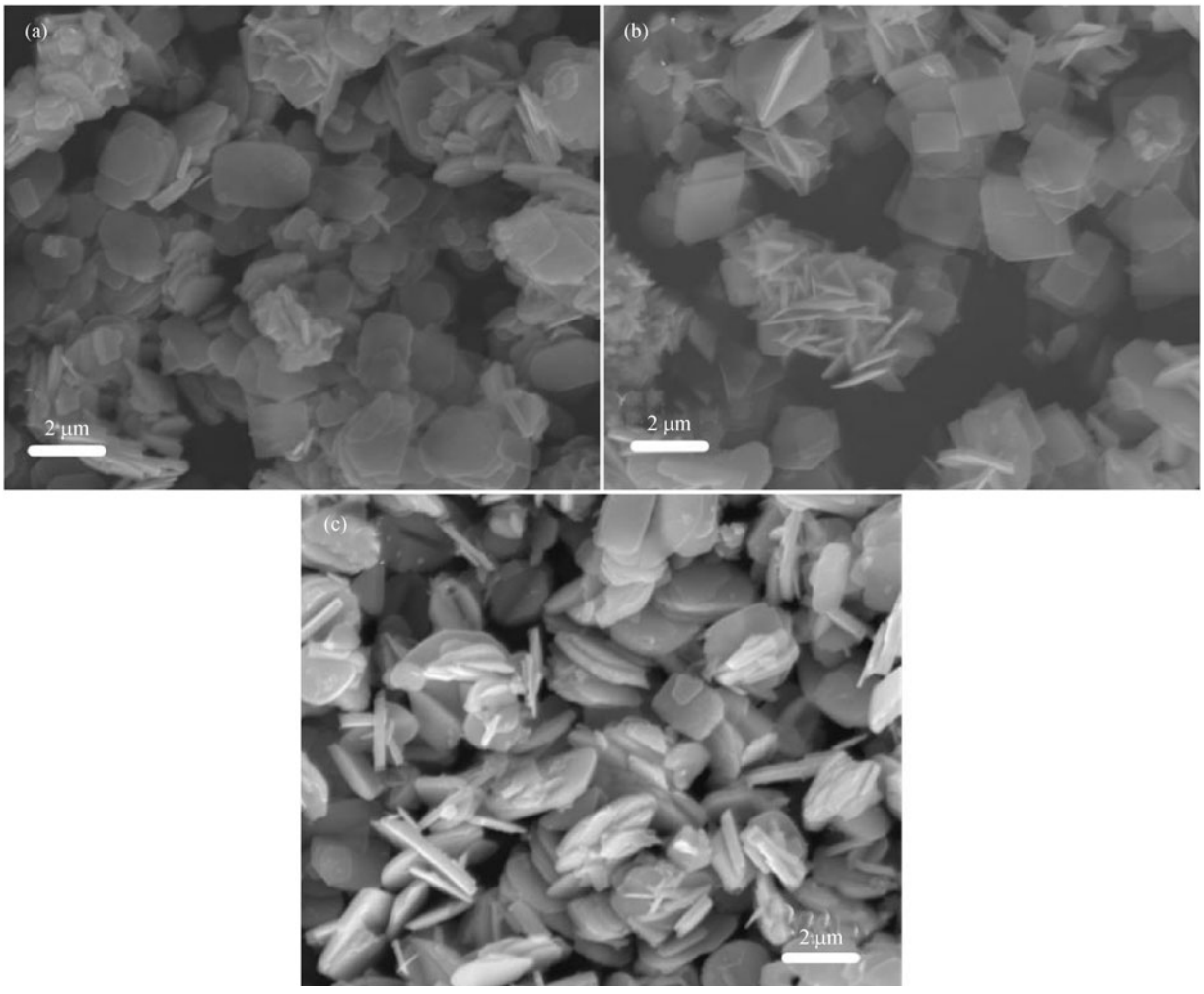


**Fig. 3** Secondary electron SEM images of $WO_3$ nanomaterials after hydrothermal treatment with a holding time of 12 h at (a) 160°C, (b) 180°C, and (c) 200°C

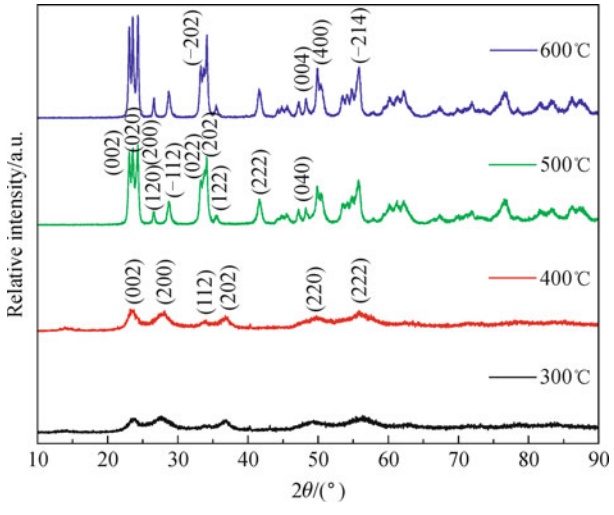


**Fig. 4** XRD patterns of $WO_3$ nanomaterials after calcination at 300°C, 400°C, 500°C and 600°C

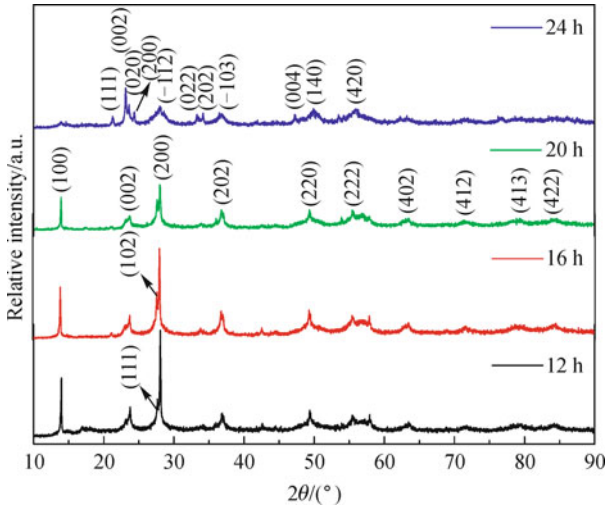


**Fig. 5** XRD patterns of $WO_3$ nanomaterials after hydrothermal treatment at holding times of 12, 16, 20, and 24 h

card No. 83-0950 [26] with $a$ = 7.3 Å, $b$ = 7.538 Å and $c$ = 7.689 Å. Liu et al. [5] found similar results for their $WO_3$ nanomaterial which was synthesized by a hydrothermal process using ammonium metatungstate and oxalic acid. Initially, their products were dried at 60°C and had a hydrate $WO_3$ ($WO_3 \cdot 0.33H_2O$) orthorhombic structure (based on XRD measurements). However, when the products were annealed at higher temperatures they transformed into hexagonal structures at 350°C and 450°C and monoclinic structures at 550°C.

Generally, the XRD patterns shown in Fig. 4 are sharper and more intense as the calcination temperature increases. At 300°C and 400°C, the peaks are broader and have lower intensities which indicates a semicrystalline material. This behavior originates from the crystalline water and volatile material in the $WO_3$. At higher temperatures, the water and volatile materials disappear. Therefore, the $WO_3$ materials calcined at 500°C and 600°C have crystalline structures as shown in their XRD patterns.

The XRD patterns for $WO_3$ calcined at 300°C and 400°C show three dominant crystalline plane orientations: (002) at $2\theta$ = 23.197°, (200) at $2\theta$ = 28.113°, and (202) at

**Table 3** Crystallite sizes of $WO_3$ nanomaterial after calcination at different temperatures

| Temperature/°C | 300 | 400 | 500 | 600 |
|---|---|---|---|---|
| Crystallite size/nm | 7.31 | 9.92 | 20.4 | 28.36 |

**Table 4** Crystallite sizes of $WO_3$ nanomaterials after hydrothermal treatment at 200°C with different holding times

| Holding time/h | 12 | 16 | 20 | 24 |
|---|---|---|---|---|
| Crystallite size/nm | 60.6 | 51.6 | 44.8 | 9.6 |

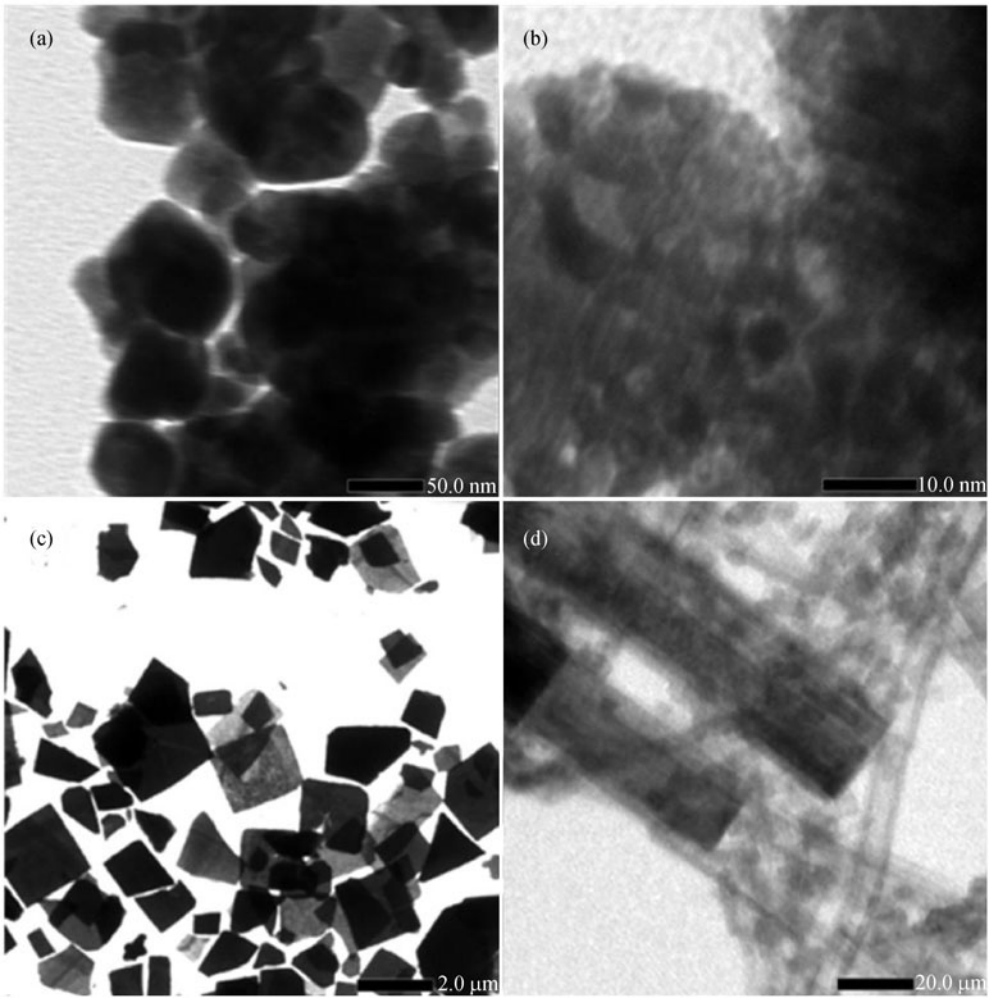


**Fig. 6** Bright-field TEM images of $WO_3$ nanomaterials (a) before and (b) after calcination at 600°C, and (c) before and (d) after hydrothermal treatment at 200°C for 12 h

$2\theta = 36.757°$, and those calcined at 500°C and 600°C also show three dominant crystalline plane orientations: (002) at $2\theta = 23.117°$, (020) at $2\theta = 23.583°$, and (200) at $2\theta = 24.367°$.

The crystallite sizes ($D$ in nm) in the materials was calculated by Scherrer formula:

$$D = \frac{0.9\lambda}{B\cos\ \theta}, \quad (1)$$

where $\lambda$ is the wavelength of the X-ray radiation (nm), $B$ is the full width at half maximum, FWHM (radian), and $\theta$ is Bragg's angle (degree) [27].

Table 3 lists the crystallite sizes of the $WO_3$ nanomaterials synthesized at different calcination temperatures. The crystallite sizes increased as temperature increased. Wang et al. [6] also found that the crystallite sizes increased with increasing calcination temperatures from 350°C, 450°C, 550°C to 650°C with sizes of 9.3, 16.4, 17.1 and 30 nm respectively.

Figure 5 shows the XRD patterns of the $WO_3$ nanomaterials after hydrothermal treatment at holding times of 12, 16, 20, and 24 h. Compared to the XRD patterns in Fig. 4, especially those for calcination at 500°C and 600°C, the intensities shown in Fig. 5 are lower. Hence the structures of the hydrothermally treated $WO_3$ are semicrystalline. The indications for this low crystallinity are more obvious at longer holding times since the peaks become broader and are less intense. This is consistent with the SEM observations in Fig. 2 which shows more irregular shapes and coagulation as the holding time increases. A hydrothermal process is a "wet" process which utilizes the moisture content in the material to generate steam which helps form the structure and shape of the material. Therefore the resulting material is still slightly "wet", even after drying which leads to a material with low crystallinity.

The change in structure from hexagonal (held for 12, 16, and 20 h) to monoclinic (held for 24 h) can be seen in

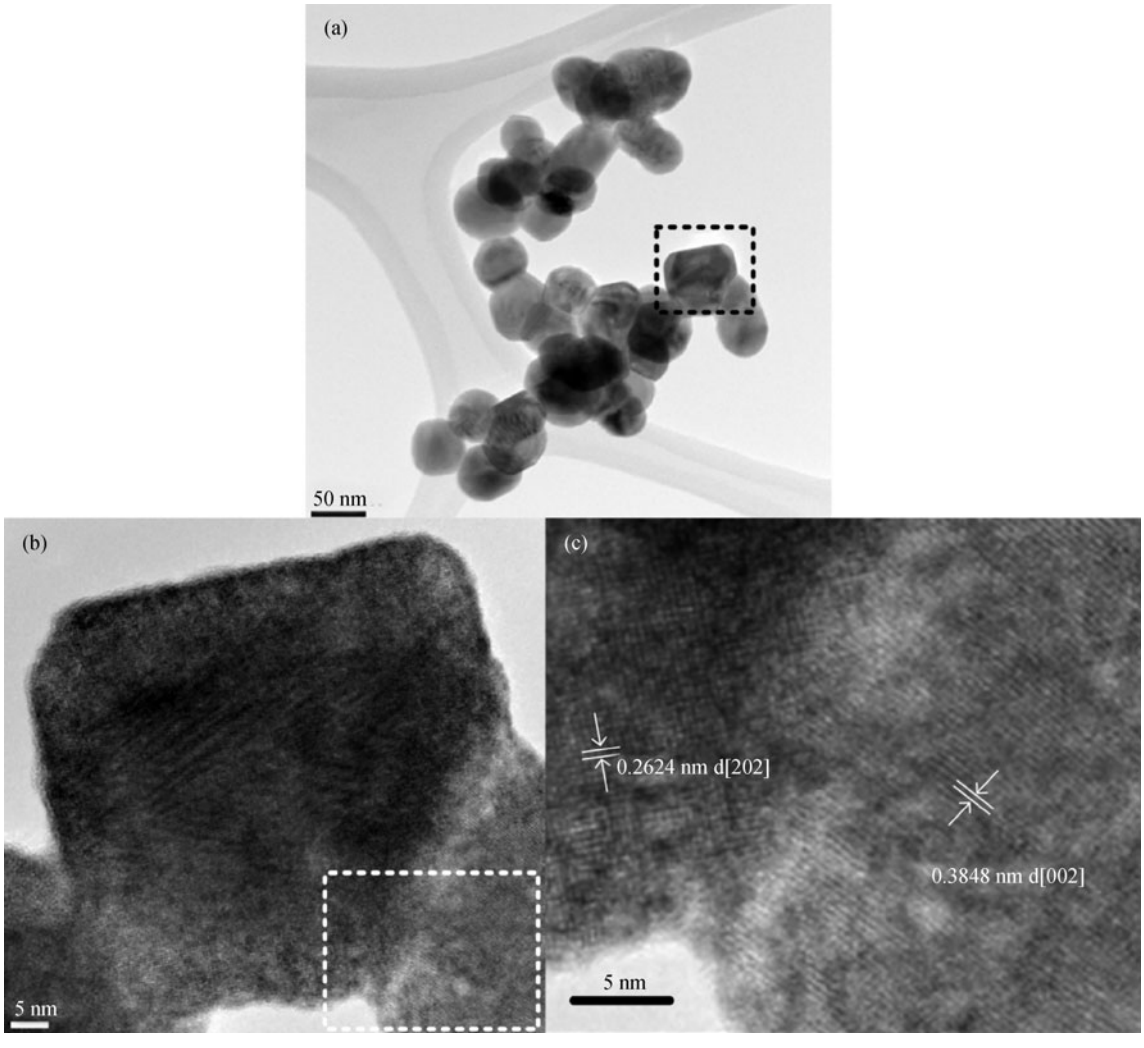


**Fig. 7** Bright-field TEM images of $WO_3$ materials calcined at 600°C. (a) a $WO_3$ cluster, (b) higher magnification of the square region in (a), (c) magnified $WO_3$ image taken from the square region in (b)

Fig. 5. The planes (100) at 13.95° and (200) at 28.113° dominate the hexagonal structure. These planes are probably reflections from the horizontal surfaces of the rectangular flakes seen in Figs. 3 and 4. A similar hexagonal structure for $WO_3$ nanomaterials has been reported by Ha et al. [14] for materials prepared from sodium tungstates, sodium or ammonium EDTA salts and sodium sulfate using a hydrothermal process at 180°C for 4 – 12 h. This hexagonal phase of $WO_3$ was first identified in the early 1980s [28].

The Scherrer formula (Eq. (1)) was employed to calculate the crystalline sizes in the samples hydrothermally treated at different holding times and the results are tabulated in Table 4. Obviously, longer holding times result in smaller crystalline sizes.

$WO_3$ has a perovskite crystal structure and displays polymorphism such as simple cubic, monoclinic, orthorhombic, triclinic, tetragonal, and hexagonal as a function of temperature [7,28,29]. As discussed above, in this research, two different $WO_3$ structures were obtained (hexagonal and monoclinic).

The stable phase of $WO_3$ at room temperature is orthorhombic or monoclinic whereas the hexagonal phase is metastable [30]. Some papers have reported different applications for the various $WO_3$ crystalline structures. For example, Liu et al. [5] used an orthorhombic $WO_3$ hydrate which changed to hexagonal and monoclinic $WO_3$ upon annealing and could then be used as an $NO_2$ gas sensor. Wang et al. [6] and Su et al. [8] obtained $WO_3$ with monoclinic structures and applied the materials as $NO_2$, acetone and alcohol gas sensors. $WO_3$ nanomaterials with triclinic structures have been synthesized and applied as electrochromic and optical devices by Deepa et al. [9] and Ozkan et al. [12], whereas those with hexagonal structures, which have open-tunnel structures and intercalation chemistry [30], have been obtained and applied as electrochemical capacitors by Chang et al. [10].

Figure 6 shows the TEM images of $WO_3$ nanomaterials before and after calcination at 600°C and before and after hydrothermal treatment at 200°C for 12 h. From Figs. 6(a) and (b), it is seen that a particle with a diameter of 10–60 nm actually consists of several smaller nanomaterials with 4–10 nm diameters. Figures 6(c) and (d) show thin rectangular transparent flakes that consist of several 10 nm × 2 μm nanotubes.

High-resolution bright-field TEM images of $WO_3$ calcinated at 600°C are shown in Fig. 7. Figure 7(a) displays a cluster of $WO_3$ nanomaterials which consists of about 37 particles with diameters of 40–100 nm. Figure 7(b) shows a higher magnification of the region inside the square in Fig. 7(a). Another region (marked with a square) in the $WO_3$ lattice in Fig. 7(b) was selected for further observation. The magnified lattice image in the square region clearly displays the lattice spacing of $WO_3$ (002), and that of $WO_3$ (202), as shown in Fig. 7(c). These results are consistent with the XRD patterns in Fig. 4 which also show (002) and (202) plane orientations.

The chemical analysis using EDX is shown in Fig. 8 and indicates that the synthesized nanomaterials contained only W and O with no impurities. The Cu signal was generated

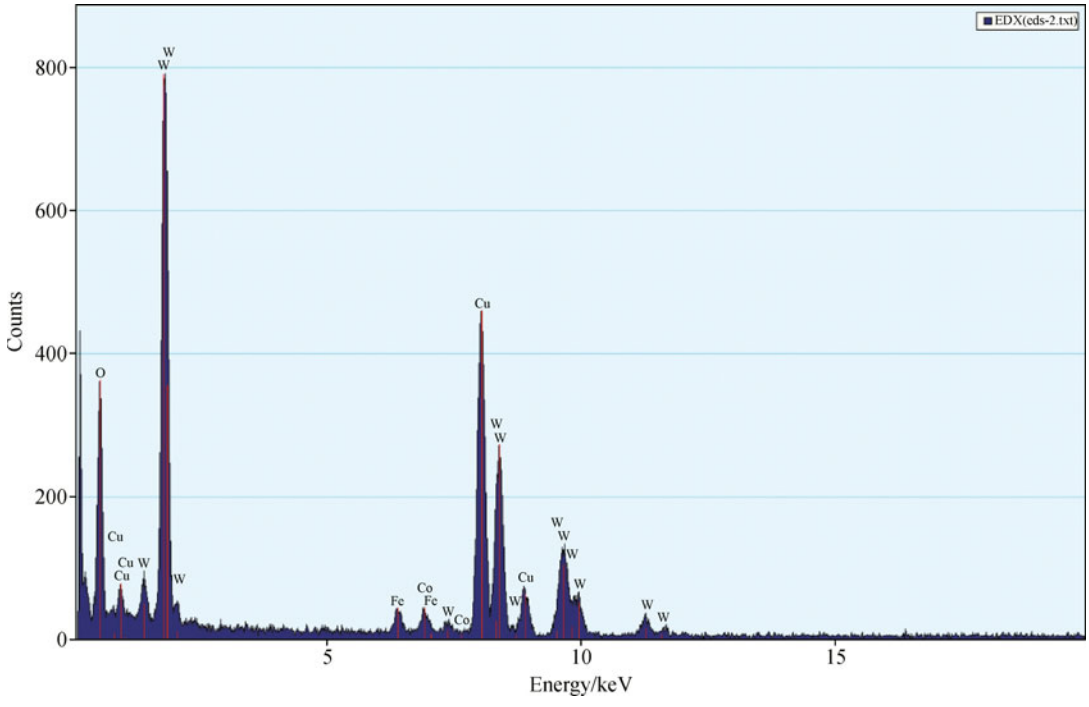


**Fig. 8** EDX spectra of $WO_3$ taken from the area in Fig. 7(a)

by copper film grid and the Fe and Co signals were generated by the TEM holder.

## 4 Summary

$WO_3$ nanomaterials with hexagonal and monoclinic phases were synthesized by a sol-gel method using $WCl_6$ and $C_2H_5OH$ precursors followed by calcination or hydrothermal treatments. The calcination and hydrothermal temperatures and the hydrothermal holding time affected the structure, morphology and size of the material. The $WO_3$ nanomaterials that were calcinated had granular shapes, whereas those that were treated hydrothermally had rectangular flake shapes. Calcination at temperatures higher than 400°C led to better crystallinity of the material and hydrothermal treatment resulted in semicrystalline materials.

**Acknowledgements** The authors gratefully acknowledge the financial and facility support from the Ministry of Research and Technology, Republic of Indonesia through Applied Research Incentive 2011(No. RT-2011-3832) and Sepuluh Nopember Institute of Technology (ITS)-Surabaya Indonesia through International Collaboration Research Grant 2011(No. 0750.042/I2.7/PM/2011).

## References

1. JCPDS Card No. 41–1230
2. Gillet M, Masek K, Gillet E. Structure of tungsten oxide nanoclusters. Surface Science, 2004, 566–568: 383–389
3. Boulova M, Gaskov A, Lucazeau G. Tungsten oxide reactivity versus $CH_4$, CO and $NO_2$ molecules studied by Raman spectroscopy. Sensors and Actuators B, Chemical, 2001, 81(1): 99–106
4. Kanan S M, Tripp C P. Synthesis, FTIR studies and sensor properties of $WO_3$ powders. Current Opinion in Solid State and Materials Science, 2007, 11(1-2): 19–27
5. Liu Z, Miyauchi M, Yamazaki T, Shen Y. Facile synthesis and $NO_2$ gas sensing of tungsten oxide nanorods assembled microspheres. Sensors and Actuators B, Chemical, 2009, 140(2): 514–519
6. Wang S H, Chou T C, Liu C C. Nano-crystalline tungsten oxide $NO_2$ sensor. Sensors and Actuators. B, Chemical, 2003, 94(3): 343–351
7. Yan A, Xie C, Zeng D, Cai S, Hu M. Synthesis, formation mechanism and sensing properties of $WO_3$ hydrate nanowire netted-spheres. Materials Research Bulletin, 2010, 45(10): 1541–1547
8. Su X, Li Y, Jian J, Wang J. In situ etching $WO_3$ nanoplates: hydrothermal synthesis, photoluminescence and gas sensor properties. Materials Research Bulletin, 2010, 45(12): 1960–1963
9. Deepa M, Singh P, Sharma S N, Agnihotry S A. Effect of humidity on structure and electrochromic properties of sol-gel-derived tungsten oxide films. Solar Energy Materials and Solar Cells, 2006, 90(16): 2665–2682
10. Chang K H, Hu C C, Huang C M, Liu Y L, Chang C I. Microwave-assisted hydrothermal synthesis of crystalline $WO_3$-$WO_3 \cdot 0.5H_2O$ mixtures for pseudocapacitors of the asymmetric type. Journal of Power Sources, 2011, 196(4): 2387–2392
11. Sun Y, Murphy C J, Reyes-Gil K R, Reyes-Garcia E A, Thornton J M, Morris N A, Raftery D. Photochemical and structural characterization of carbon-doped $WO_3$ films prepared via spray pyrolysis. International Journal of Hydrogen Energy, 2009, 34(20): 8476–8484
12. Ozkan E, Lee S H, Liu P, Tracy C E, Tepehan F Z, Pitts J R, Deb S K. Electrochromic and optical properties of mesoporous tungsten oxide films. Solid State Ionics, 2002, 149(1–2): 139–146
13. Su L, Lu Z. All solid-state smart window of electrodeposited $WO_3$ and $TiO_2$ particulate film with PTREFG gel electrolyte. Journal of Physics and Chemistry of Solids, 1998, 59(8): 1175–1180
14. Ha J H, Muralidharan P, Kim D K. Hydrothermal synthesis and characterization of self-assembled h-$WO_3$ nanowires/nanorods using EDTA salts. Journal of Alloys and Compounds, 2009, 475 (1–2): 446–451
15. Pyper O, Schollhorn R, Donkers J J T M, Krings L H M. Nanocrystalline structure of $WO_3$ thin films prepared by the sol-gel technique. Materials Research Bulletin, 1998, 33(7): 1095–1101
16. Yous B, Robin S, Donnadieu A. Chemical vapor deposition of tungsten oxides: a comparative study by XPS, XRD and RHEED. Materials Research Bulletin, 1984, 19(10): 1349–1354
17. Pyun S I, Kim D J, Bae J S. Hydrogen transport through r.f. magnetron sputtered amorphous and crystalline $WO_3$ films. Journal of Alloys and Compounds, 1996, 244(1-2): 16–22
18. Abdullah S F, Radiman S, Hamid M A A, Ibrahim N B. Effect of calcinations temperature on the surface morphology and crystallinity of tungsten (VI) oxide nanorods prepared using colloidal gas aphrons method. Colloids and Surfaces A: Physicochemical and Engineering Aspects, 2006, 280: 88–94
19. Hidayat D, Purwanto A, Wang W N, Okuyama K. Preparation of size-controlled tungsten oxide nanoparticles and evaluation of their adsorption performance. Materials Research Bulletin, 2010, 45(2): 165–173
20. Deki S, Beleke A B, Kotani Y, Mizuhata M. Synthesis of tungsten oxide thin film by liquid phase deposition. Materials Chemistry and Physics, 2010, 123(2–3): 614–619
21. Houx N L, Pourroy G, Camerel F, Comet M, Spitzer D. $WO_3$ nanoparticles in the 5–30 nm range by solvothermal synthesis under microwave or resistive heating. Journal of Physical Chemistry B, 2010, 114(1): 155–161
22. Brinker C J, Scherer G W. Sol-Gel Science: The Physics and Chemistry of Sol-Gel Processing. London: Academic Press Inc, 1990, 2: 47–49
23. Chai F, Tan R, Cao F, Zhai F, Wang X, Shao C, Liu Y. Dendritic and tubular tungsten oxide by surface sol–gel mineralisation of cellulosic substance. Materials Letters, 2007, 61(18): 3939–3941
24. Huirache-Acuña R, Paraguay-Delgado F, Albiter M A, Lara-Romero J, Martínez-Sánchez R. Synthesis and characterization of $WO_3$ nanostructures prepared by an aged-hydrothermal method. Materials Characterization, 2009, 60(9): 932–937
25. JCPDS Card No. 85–2459
26. JCPDS Card No. 83–0950
27. Cullity B D, Stock S R. Elements of X-ray Diffraction. 3rd ed. London: Prentice Hall, 2001, 170
28. Ramana C V, Utsunomiya S, Ewing R C, Julien C M, Becker U. Structural stability and phase transitions in $WO_3$ thin films. Journal

of Physical Chemistry B, 2006, 110(21): 10430–10435

29. Chatten R, Chadwick A V, Rougier A, Lindan P J D. The oxygen vacancy in crystal phases of $WO_3$. Journal of Physical Chemistry B, 2005, 109(8): 3146–3156

30. Szilágyi I M, Madarász J, Pokol G, Király P. Tárkányi , Saukko S, Mizsei J, Tòth A L, Szabò A, Varga-Josepovits K. Stability and controlled composition of hexagonal $WO_3$. Chemistry of Materials, 2008, 20(12): 4116–4125